JOURNAL OF Applied Polymer SCIENCE

Effect of titanium dioxide (TiO_2) distribution and minute amounts of carbon black on the opacity of PVDF based white composite films

Tongbing Li,[1,2] Dekun Sheng,[1] Zhengrong Xiong,[1] Xiumei Gao,[1,2] Fance Ji,[1,2] Yuming Yang[1]

[1]Polymer Composites Engineering Laboratory, Changchun Institute of Applied Chemistry, Chinese Academy of Sciences, 5625 Renmin Street, Changchun, 130022, People's Republic of China

[2]University of the Chinese Academy of Sciences, No.19A Yuquan Road, Beijing, 100049, China

Correspondence to: Y. Yang (E-mail: ymyang@ciac.ac.cn)

ABSTRACT: There is a contradiction in making completely opaque and white plastic film with a required high TiO_2 filling fraction, which resulted in inefficient pigment utilization and high cost. Two methods were used here to overcome the contradiction. Firstly, TiO_2 was grafted with poly(methyl methacrylate) (PMMA) by atom transfer radical polymerization to improve the pigment dispersion in poly(vinylidene) fluoride (PVDF). Secondly, minute amounts of carbon black (CB) were added into the PMMA-*g*-TiO_2/PVDF system to enhance opacity and decrease TiO_2 fraction. The structure, morphology, and properties of PMMA-*g*-TiO_2 hybrid particles and composite films were investigated by FTIR, TEM, TGA, SEM, DMA, covering power meter, and UV/VIS spectrophotometer, etc. It was observed that PMMA-*g*-TiO_2 was dispersed uniformly as individual particles in PVDF due to the good compatibility between PMMA and PVDF. Therefore, the opacity of PMMA-*g*-TiO_2/PVDF films was markedly higher than unmodified-TiO_2/PVDF ones. Adding minute amounts of CB can significantly increase the opacity of the thin film due to its absorption effect on decreasing light transmittance. The contrast ratio (CR) of the PMMA-*g*-TiO_2/PVDF film with 20 μm thickness and 25 vol % TiO_2 was 97.67%, lower than the critical CR 98% for a complete opacity, however, the CR of sample with 10 vol % TiO_2 was 98.1% as the CB concentration was 2×10^{-4} g/cm^3, saved more than 15% TiO_2. We proposed that a critical thickness d_0 existed for the CB/PMMA-*g*-TiO_2/PVDF composite films, under which the light reflectance increased as a function of thickness, otherwise, the reflectance kept constant. Besides, d_0 could be decreased by increasing CB concentration. © 2015 Wiley Periodicals, Inc. J. Appl. Polym. Sci. **2016**, *133*, 43064.

KEYWORDS: carbon black and opacity; films; light scattering; titanium dioxide

Received 7 September 2015; accepted 18 October 2015

DOI: 10.1002/app.43064

INTRODUCTION

White films or coatings have the ability to partially or totally obscure the objects they cover. This hiding power is defined as the opacity which is usually measured as contrast ratio (CR). Opacity is a desired property for imparting a white surface appearance and obscuring or protecting against the deleterious effect of light. Therefore, the white completely opaque plastic films have a widespread commercial importance in applications, such as airship envelope materials and photovoltaic back-sheet protection. However, most studies into opacity were focused on the coatings or paints not on the plastic films, which have different applications and manufacturing process. The opacity and the white appearance of white films derived from the fact that the incident light is reflected. This reflection results from the scattering of light by the pigment particles embedded in the medium. The scattered light deflected from the incident direction, so the large number of successive scattering, named by multiple scattering, ultimately causes part of the incident light to return to the viewer's eye. Therefore, a higher scattering efficiency means a better opacity. The scattering efficiency of pigment particles is directly dependent on the contrast of refractive index between pigment and the surrounding medium. The larger the contrast, the stronger is the amplitude of the scattering events. For this reason, rutile titanium dioxide (TiO_2) becomes the most important and common white pigment, for it has the highest refractive index of 2.8 among all the white pigments. Particle size is another important factor to dominate the scattering efficiency. Many theory and experimental studies have shown that a maximum scattering strength occurs when the particle diameter is about half of the wavelength of incident light.[1] As a result, many commercial TiO_2 grades now have a size distribution as narrow as technically possible and centered about 0.25 μm in diameter to maximize scattering.[2] In addition to the refractive index and particle size, inter-particle separation is a third important parameter to influence the pigment scattering efficiency, which is dependent on the spatial dispersion state

and the filling fractions of the pigments. When particles get close to a certain degree, the scattering efficiency will decrease as the inter-particle separation decreased, which is called crowding effect or dependent scattering effect.[2–5] Theory studies has concluded that, the dependent scattering effect can be neglected when the center-to-center separation is greater than two or three diameter, otherwise, it will be significant as the separation decreases.[4] In practice, the pigment particles tend to form clusters or agglomerations in the matrix for the big specific surface energy and so the inter-particle distance is very small in the clusters or agglomerations. As a result, improving the pigment dispersion state has a great significance in improving the particle scattering efficiency. In order to overcome the problem of agglomerations and improve the dispersion to some extent, some strategies were carried out such as very low TiO_2 filling fractions was used, surface chemical modification by coupling agent or other low molecular dispersant.[6–10] In addition, there is a controversial view that nano-particle fillers can act as "spacers" to inhibit the agglomeration of TiO_2 pigment and improve scattering efficiency and opacity, both in experimental and theory studies.[11–15] By now, few studies have achieved the ideal individual particle dispersion, especially at high volume concentrations. In the field of nanocomposites, grafting some kind of polymer with a good compatibility with the matrix polymer onto nanoparticles is an effective and common method to improve their dispersion. However, the same approach has not been used in the dispersion of pigmentary TiO_2.[16–23] It is expected that the ideal pigment dispersion can be achieved as the pigmentary TiO_2 were grafted with polymers even at high filling fractions, and the theoretical relations between particle separation, dependent scattering and the opacity can be studied more exactly. As to the filling fraction of TiO_2, there is a well-known relationship to depict the opacity as a function of pigment volume concentrations (PVCs).[12] The opacity increases first, however, the increment gradually decreased because of the growing dependent scattering effect decreases the scattering efficiency of TiO_2. It implies that the higher TiO_2 filling fraction is needed in the formulation to reach a non-negligible enhancement of the overall opacity, which means lower TiO_2 utilization efficiency, higher manufacture cost, and worse mechanical properties. This contradiction will be very serious when the practical required film thickness is as thin as no more than 30 μm, which needs a high TiO_2 filling fraction to realize a complete opacity. As the PVCs further increases the opacity gradually decreases until the critical pigment volume concentration (CPVC) for the more serious lose of pigment scattering efficiency. When the concentration exceeds the CPVC the opacity increases again due to formation of voids, but voids are unwanted in the plastic film due to their adverse effect on the mechanical properties. In the past decades, most studies on the opacity were focused on the TiO_2/polymer systems without absorption effect, in which the opacity is derived only from the scattering effect of TiO_2 pigment. However, few studies worked on the system with both scattering and absorption effect. Focke *et al.*[24] built a theoretical lattice model, and indicated that the hiding power of black pigmentation is significantly higher than white pigmentation at equivalent concentrations and absorbing entities can have a significant effect on the opacity of white films according to the numerical calculation. Therefore, it is rational to expect that the combination of scattering and absorption effect is an effective way to manufacture completely opaque white thin film with lower TiO_2 concentrations, which means a higher TiO_2 utilization efficiency.

In this article, the poly(vinylidene) fluoride (PVDF) was selected as the matrix polymer with advantages including good stability to rigorous temperatures, UV exposure, aggressive chemical environments, and excellent mechanical properties, which render it a good candidate as protective layer of the airship envelope materials.[25–28] Poly(methyl methacrylate) (PMMA) was grafted onto the TiO_2 particle to improve the pigment dispersion because of the good compatibility between PMMA and PVDF.[29–35] Then the effect of the dispersion on the opacity was investigated at a wide filling fraction range. Minute amounts of carbon black (CB) were incorporated into the PMMA-*g*-TiO_2/PVDF composite, and the influence of absorption effect on the opacity and other optical properties of the composite film were deeply studied.

EXPERIMENTAL

Materials

The PVDF resin used in this experiment was Solef® 6010PVDF homopolymer, Solvay Solexis Co. Ltd. TiO_2 (Tiona RCL69) was obtained from Milleddium Co., the United States. CB (660R) was obtained from CABOT Co., the United States. Methyl methacrylate (MMA) was purchased from Aladdin. MMA (Merck, Mumbai)was purified by distillation over CaH_2 under reduced pressure and stored under N_2 atmosphere prior to use in the polymerization reaction. 3-Aminopropyltriethoxy silane (APTES) (Aldrich), pentamethyldiethylenetriamine (PMDETA) (Aladdin), 2-bromoisobutyryl bromide (Aladdin), and Cu(I)Br (Aladdin) were used without any further purification. N,N-Dimethylformamide (DMF), pyridine, and triethanolamine were in analytical reagent grade and were used as received. Toluene was distilled over metallic sodium.

Synthesis of PMMA-*g*-TiO_2 via Atom Transfer Radical Polymerization (ATRP)

About 20 g of TiO_2 pigment and 2 mL of triethanolamine were dispersed in 500 mL of ethanol. The mixture were stirred and dispersed by ultrasonic for 60 min at room temperature and then heated to 50°C. Then, 20 mL APTES were added drop by drop. The mixture were stirred using a magnetic bar at 50°C for 24 h. Then, the products were purified by repeating centrifugal sedimentation and re-dispersion of the sediment in absolute ethanol for five times to remove any unreacted silane coupling and triethanolamine. The APTES modified TiO_2 (represented as TiO_2-NH_2) particles were obtained after being dried under vacuum. The obtained TiO_2-NH_2 particles, 500 mL of anhydrous toluene and 4 mL of pyridine were added into a 1000 mL flask. The mixture were stirred and dispersed by ultrasonic for 30 min at room temperature, and then 5 mL of 2-bromoisobutyryl bromide was added dropwise at 0°C. The mixture was stirred for 1 h at 0°C, followed by stirring at room temperature for 12 h. The resultant brominated TiO_2 particles (represented as TiO_2-Br) were obtained after repeating centrifugal

sedimentation and redispersion of the sediment in toluene for five times to remove any unreacted 2-bromoisobutyryl bromide. About 5 g of TiO_2-Br, 0.22 g of CuBr, were placed into a three-necked, round-bottomed flask equipped with a magnetic stir bar, condenser, and sealed with a rubber plug. The flask was evacuated and back-filled with N_2 gas for three times to remove any trace of oxygen. Then 100 mL of MMA and 200 mL of DMF was injected into the flask through syringe. The mixture were stirred and dispersed by ultrasonic for 30 min. After refrigeration in freezing brine for 0.5 h, the flask was evacuated and back-filled with N_2 gas for three times to remove any trace of oxygen. Then 0.48 mL PMDETA was injected into the flask through syringe .The flask was immersed in oil bath at 60°C immediately and kept stirring for 12 h. The final products were purified by repeating centrifugal sedimentation and redispersion of the sediment in ethyl acetate for five times to ensure the complete removal of the resultant homopolymers. PMMA-*g*-TiO_2 hybrid was obtained after a further drying at 70°C under vacuum for 72 h.

Fabrication of PVDF Based Composite Films

Four kinds of PVDF based composite film were fabricated by solution casting method, pure PVDF film, unmodified-TiO_2/PVDF composite film, PMMA-*g*-TiO_2/PVDF composite film and CB/PMMA-*g*-TiO_2/PVDF composite film. The solutions were prepared as follows: (1) for pure PVDF system, 1 g (0.57 cm^3) PVDF was added into 10 mL DMF solvent, the mixture was stirred for 1 h at 50°C and a homogeneous solution was obtained. (2) For unmodified-TiO_2/PVDF system, TiO_2 was dispersed into 10 mL DMF first and ultrasonicated for 30 min. After that, PVDF was added into the solution, the mixture was stirred for 1 h at 50°C and a homogeneous suspension was obtained. According to the different TiO_2 volume fraction (1%, 3%, 5%, 10%, 15%, 20%, and 25%) relative to the total volume of TiO_2 and PVDF (0.57 cm^3), the samples were named Vp1, Vp3, Vp5, Vp10, Vp15, Vp20, and Vp25, respectively. (3) For PMMA-*g*-TiO_2/PVDF system, PMMA-*g*-TiO_2 was dispersed into 10 mL DMF first by magnetic stirring 12 h under 50°C, then, the suspension was ultrasonicated for 10 min. After that, PVDF was added into the solution, the mixture was stirred for 1 h at 50°C and a homogeneous suspension was obtained. According to the different TiO_2 volume fraction (1%, 3%, 5%, 10%, 15%, 20%, and 25%) relative to the total volume of PMMA-*g*-TiO_2 and PVDF (0.57 cm^3), the samples were named V1, V3, V5, V10, V15, V20, and V25, respectively. (4) For CB/PMMA-*g*-TiO_2/PVDF system, PMMA-*g*-TiO_2 was first dispersed into 10 mL DMF solvent by magnetic stirring 12 h under 50°C, then CB was added into the dispersion, and the suspension was ultrasonicated for 10 min. After that, PVDF was added into the solution, the mixture was stirred for 1 h at 50°C and a homogeneous suspension was obtained. The TiO_2 volume fraction relative to the total volume of PMMA-*g*-TiO_2 and PVDF (0.57 cm^3) was 10%. According to the different CB concentration relative to solid constituent (0.57 cm^3), such as 1×10^{-4} g/cm^3, 2×10^{-4} g/cm^3, 4×10^{-4} g/cm^3 the samples were named V10-1, V10-2, and V10-4, respectively. The composite films were fabricated by pouring the suspension onto glass substrate which kept in horizontal level and coating with a casting knife. The prepared wet coating were carefully evaporated at 60°C in an oven for 30 min, then, heated to 190°C by 5°C/min to remove any remaining traces of the solvent and then cooled down to room temperature naturally. The thickness of the films was controlled through the slit height of the casting knife.

Characterizations

Microscopy. The morphology of PMMA-*g*-TiO_2 and pristine TiO_2 particles were studied using a transmission electron microscope (TEM) (JEOL JEM-1011) operated at an acceleration voltage of 200 kV. A drop of the dilute solution of the homogeneous PMMA-*g*-TiO_2/DMF suspension on the carbon coated copper grid was initially dried in air at 30°C and finally dried under vacuum at 30°C for 2 days. Scanning electron microscopy (SEM) images about dispersion state of PMMA-*g*-TiO_2 and pristine TiO_2 particles in PVDF matrix were obtained using an XL30ESEM-FEG scanning electron microscope at an acceleration voltage of 20 kV. The samples were coated by gold.

Spectroscopy. Fourier transform infrared (FTIR) spectra of pristine and grafted TiO_2 were obtained on a Perkin Elmer 1600 spectrometer. Dried solids were pressed with KBr and the discs were scanned in the range of 4000–400 cm^{-1} with a resolution of 2 cm^{-1}.

Thermal Study. Thermogravimetric analysis (TGA) traces were obtained on a Perkin Elmer Pyris 6 thermogravimetric analyzer with a heating rate of 10°C/min[1] over the temperature range of 30°C–700°C under the dry flow of O_2 at the rate of 20 mL/min[1].

Gel Permeation Chromatography (GPC) Characterization. The molecular weight and molecular weight distribution were determined by GPC equipped with a 5 mm MIXED-C PL gel column (300 × 7.5 mm). Polystyrene was used as a calibration standard and DMF as the eluent with a flow rate of 1.00 mL/min.

Dynamic Mechanical Property. Dynamic mechanical tests were performed on a DMA/SDTA861[e] (Mettler Toledo) in tension mode. The samples were installed on the small tension clamp of the calibrated instrument. The samples were heated from −80°C to 125°C at a heating rate of 3°C/min. The storage modulus, loss modulus, and tan δ values were measured at a constant frequency of 1 Hz, force amplitude value of 5 N, and displacement amplitude value of 10 μm.

Optical Properties. The CR is a common and simple index to evaluate the opacity of film, which is defined as:

$$CR = \frac{R_b}{R_w} \times 100\%$$

where R_b and R_w are the reflectance of the film measured on, respectively, black and white substrates.[36] It is assumed that when the CR reaches 98%, the human eye cannot distinguish any further changes in opacity.[2] The TAPPI opacity of the PVDF based composite films was measured using a covering power meter (C84-III) with a quartz tungsten-halogen lamp filtered for illumination at 572 nm. Five different sites were measured and the average value was achieved as the final value. Film thickness was measured using a screw micrometer.

Scheme 1. Fabrication procedure of the composite film. [Color figure can be viewed in the online issue, which is available at wileyonlinelibrary.com.]

Measurements of the diffuse reflectance and diffuse transmittance of the films were made by using a Labsphere model RSA-PE-19 on a Perkin–Elmer Lambda 950 UV/VIS spectrophotometer with reflectance spectroscopy accessory (integrating sphere). The instrument is a dual-beam one, and uses a halogen lamp for illumination at wavelengths longer than 319 nm and a deuterium lamp at shorter wavelengths. Data were acquired over the wavelength range of 400–800 nm. The scan rate was 100 nm/min, and data were taken at 1 nm intervals. The nominal band pass was 2 nm, corresponding to an actual spectral bandwidth ranging from 2.02 nm at short wavelengths to 1.69 nm at long wavelengths. For transmittance measurements the light was directly incident on the composite film sample, and nothing was placed in the reference beam.

Mechanical Property. Tensile tests were carried out on solvent cast films of uniform thickness using a universal testing machine (Instron 1121 testing machine) at a strain rate of 5 mm/min at room temperature (30°C). At least five samples of each type were drawn to fracture to observe the reproducibility.

RESULTS AND DISCUSSION

Synthesis and Characterization of PMMA-*g*-TiO_2 Hybrid Particles

The PVDF based composite films were fabricated by solution casting, as shown in Scheme 1. The detailed fabrication procedure is shown in the "Experimental" section. First, the TiO_2 pigment was grafted with PMMA via ATRP. FTIR measurement is a useful method to confirm the successful synthesis of PMMA-*g*-TiO_2. Figure 1 shows the FTIR spectra of pristine and grafted TiO_2. In the spectrum of pristine TiO_2 [Figure 1(a)], the appearance of a strong peak at low frequencies (below 900 cm^{-1}) is due to the vibration absorbance from Ti—O/O—O bonds in TiO_2 lattice. The broad peak between 3200 and 3600 cm^{-1} are due to the stretching vibrations of the —OH group on the surface of TiO_2 particles. In Figure 1(b), there was a peak at 1130 cm^{-1} corresponding to the Si—O stretching frequency, which conform to the binding of ethoxy functional groups in 3-APTS to the free hydroxyl groups on TiO_2 surface. The characteristic absorption peaks of amide groups, C═O bond and N—H bond stretching vibration, appeared at 1633 cm^{-1} and 1527 cm^{-1} in the FTIR spectrum of TiO_2—Br, respectively [Figure 1(c)]. This confirm to the immobilization of 2-bromoisobutyryl groups onto the surface of TiO_2. Compared with the TiO_2-Br, the FTIR spectrum of PMMA-*g*-TiO_2 [Figure 1(d)] shown several new adsorption peaks. The sharp peak at 1730 cm^{-1} is assigned to the C═O bond stretching vibration of PMMA. The peaks at 2994 cm^{-1} and 2948 cm^{-1} are corresponding to C—H bond stretching vibrations of the CH_3 and CH_2 groups of grafted PMMA. In addition, the characteristic peaks in 1150–1250 cm^{-1} region are corresponding to the stretching vibrations of C—O—C in PMMA. These results indicate that PMMA was grafted successfully onto the surface of TiO_2 through ATRP reaction. Furthermore, the peak around 3429 cm^{-1} is assigned to the stretching vibration of hydroxyl groups, which suggests the residue of hydroxyl groups on the surface of TiO_2 after the grafting modification.

The successful modification of TiO_2 particles by ATRP can also be proved by morphological evidences by comparing TEM images of unmodified-TiO_2 and PMMA-*g*-TiO_2 particles as indicated in Figure 2. The black area was attributed to TiO_2. Compared with unmodified-TiO_2 particles [Figure 2(a)], TiO_2 particles in PMMA-*g*-TiO_2 [Figure 2(b)] appeared a new gray

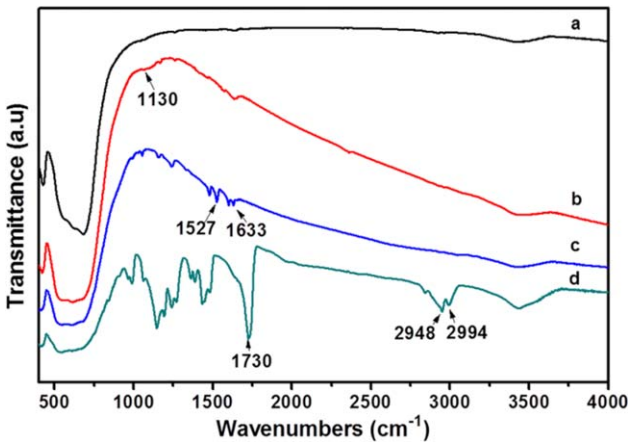

Figure 1. FTIR spectra of (a) unmodified-TiO_2, (b) TiO_2-NH_2, (c) TiO_2-Br, and (d) PMMA-*g*-TiO_2. [Color figure can be viewed in the online issue, which is available at wileyonlinelibrary.com.]

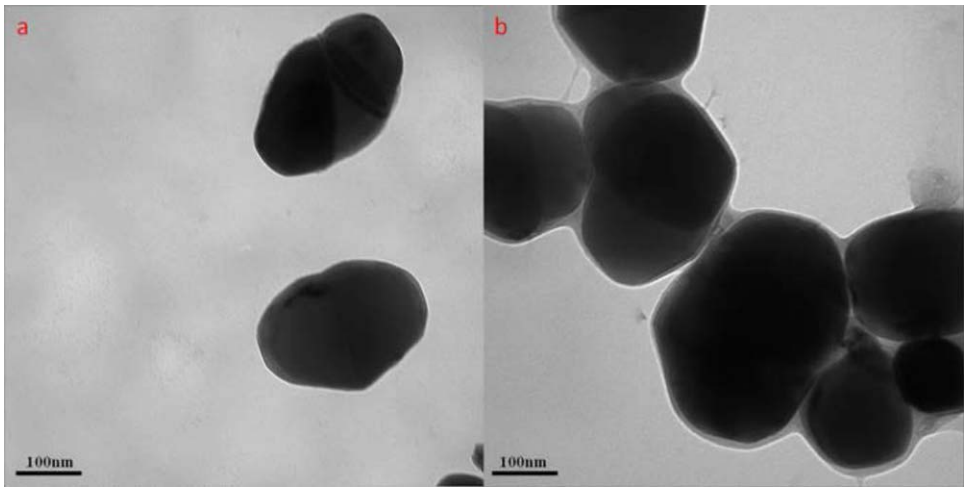

Figure 2. Representative TEM images of unmodified-TiO_2 (a), and PMMA-*g*-TiO_2 (b). [Color figure can be viewed in the online issue, which is available at wileyonlinelibrary.com.]

shell area with the thickness around 10 nm, which arise from the grafted PMMA.

The TGA results shown in Figure 3 demonstrate the grafting ratio of initiator and PMMA. The difference in weight loss between unmodified-TiO_2 and surface-grafted TiO_2 was ascribed to the amount of grafted organic compounds. As shown in Figure 3(a), the pristine TiO_2, which was dried at 100°C under vacuum for 24 h, displays no weight loss through the whole experimental temperatures. Instead, TiO_2—Br shows weight loss of 5.77 wt % in Figure 3(b). The thermogram of PMMA-*g*-TiO_2 [Figure 3(c)] exhibited a major decomposition event at about 350°C, which was due to the decomposition of grafted PMMA. The whole grafting ratio of the TiO_2 was 23.06 wt % [Figure 3(c)], so the grafted PMMA content on TiO_2 surface estimated by the weight loss was nearly 17.29 wt %.

Gel permeation chromatography (GPC) was employed to determine the relative molecular weight (M_n) and molecular weight distribution (M_w/M_n) of PMMA grafted from the TiO_2 surface (the polymer was cleaved from the TiO_2 surface with hydrofluoric acid). From the GPC result shown in Figure 4, it can be seen that the value of M_n is 244,652 g/mol and M_w/M_n is 1.90. The molecular weight distribution is unimodal and relative narrow, indicating that the ATRP process is performed in a controlled manner. The relatively high molecular weight facilitates the dispersion stability of PMMA-*g*-TiO_2 in the PVDF/DMF solution which resulted in the good pigment distribution and good mechanical properties of the composite film.

The Structure and Morphology of the PVDF Based Composite Films

Figure 5 shows the SEM micrographs of the fracture surface and film surface of the unmodified-TiO_2/PVDF and PMMA-*g*-TiO_2/PVDF composite films, and the results demonstrated the disperse state of TiO_2 particles in the bulk phase and surface layer. The effect of surface modification on the dispersion of TiO_2 can be revealed by a representative comparison between the samples of Vp10 and V10. For Vp10 [Figure 5(a1,a2)], it is observed that most of the particles dispersed in the form of

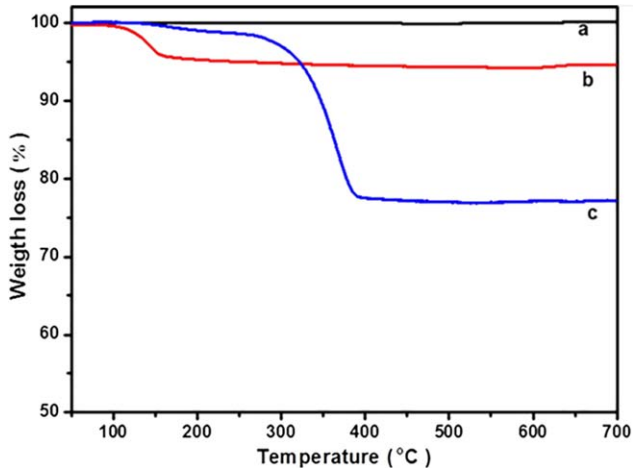

Figure 3. TGA curves for (a) unmodified-TiO_2, (b) TiO_2-Br, and (c) PMMA-*g*-TiO_2. [Color figure can be viewed in the online issue, which is available at wileyonlinelibrary.com.]

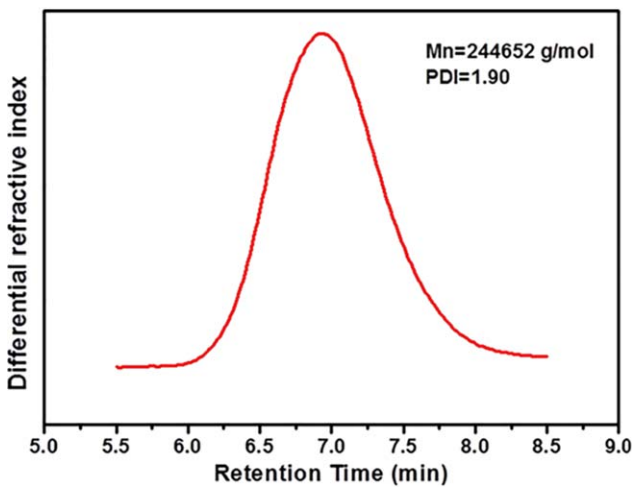

Figure 4. GPC curve of grafted PMMA after the cleavage. [Color figure can be viewed in the online issue, which is available at wileyonlinelibrary.com.]

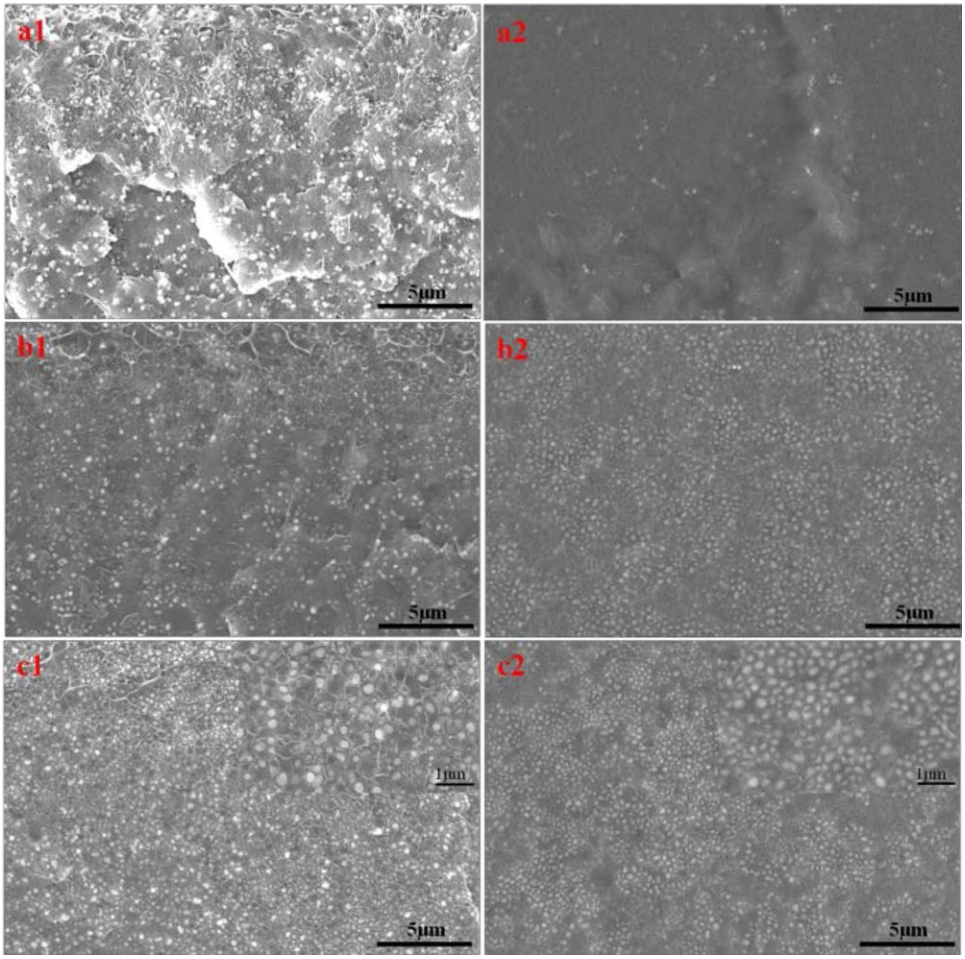

Figure 5. SEM images of the fracture surface of Vp10 (a1), V10 (b1), V25 (c1) and film upper surface of Vp10 (a2), V10 (b2), V25 (c2). [Color figure can be viewed in the online issue, which is available at wileyonlinelibrary.com.]

clusters or agglomerations both in the bulk phase and the surface layer of the composite film. (Similar dispersion state can be seen in the other samples and it became worse at higher concentrations, which are not shown here.) As to V10 [Figure 5(b1,b2)], however, a completely different picture can be seen that almost all of the TiO_2 particles dispersed uniformly as individual particle both in the bulk phase and in the surface layer. These results proved that surface modification improved the dispersion of TiO_2 in the PVDF because of the good compatibility between PMMA and PVDF.[29–32] For V20 (Figure 5(c1,c2)], we can see that the same excellent dispersion maintained as the TiO_2 concentration reached up to 20%. In the magnification images inserted, it can be found that each TiO_2 particles was wrapped by the matrix polymer, which further displayed the excellent affinity between PMMA-*g*-TiO_2 and PVDF.

The good dispersion of particles in the polymer can be further testified by the dynamic mechanical analysis (DMA) measurement, which is an effective method to investigate the microstructure of the polymer and composites by measuring the glass transition temperature (T_g). In addition to tan δ, the loss modulus (E'') indicating the energy lost as heat is another parameter to determine T_g. Figure 6 shows the E''–temperature plots for pure PVDF, unmodified, and PMMA grafted TiO_2/PVDF composite films. The curve of pure PVDF exhibited only one transition (denoted as TrI) around −35°C, which was the T_g of the PVDF. However, a new peak appeared around 60°C and its area

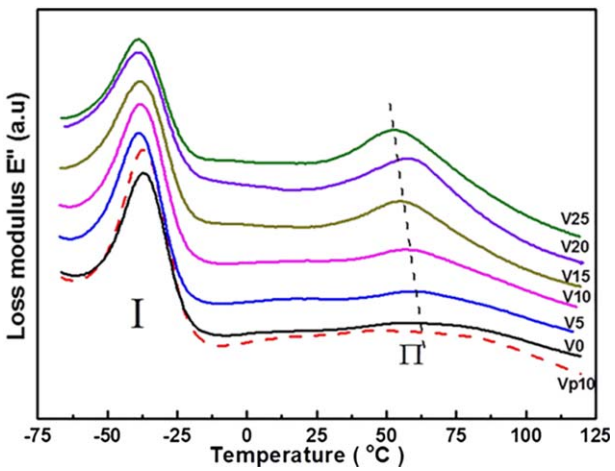

Figure 6. Variation of loss modulus as a function of temperature for PVDF based composites films: V0 (Pure PVDF), V5, V10, V15, V20, V25, and Vp10. [Color figure can be viewed in the online issue, which is available at wileyonlinelibrary.com.]

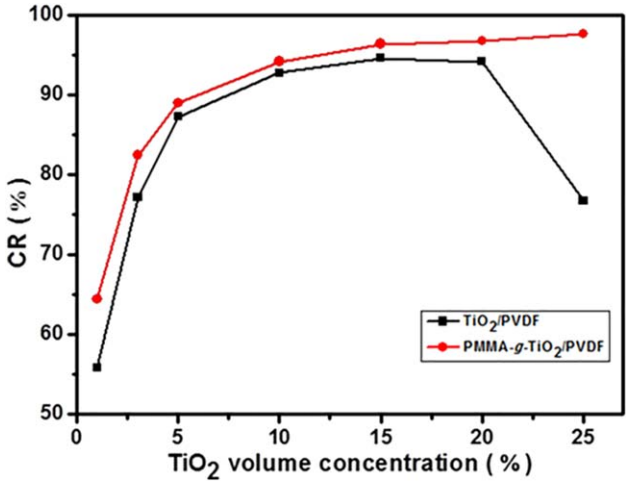

Figure 7. Effect of dispersion state and PVCs on the CR when the thickness of film is 20 μm. The *dashed line* represents 98% CR. [Color figure can be viewed in the online issue, which is available at wileyonlinelibrary.com.]

became lager as the amount of PMMA-*g*-TiO_2 incorporated into the PVDF increased. This new peak (TrII) was attributed to the glass transition of the mixed amorphous phase of PVDF and PMMA.[37–39] (The new peak was not very clear in the sample of V1 and V3 for the very small amount of the mixed phase.) It is reasonable to speculate that this mixed phase existed as the interphase between the TiO_2 and PVDF matrix and played a role of improving the affinity of TiO_2 to PVDF and preventing a direct contact between TiO_2 particles. The curve of Vp10 was nearly identical with pure PVDF without any new peak appears around 60°C (the other samples of unmodified-TiO_2/PVDF composites exhibited the similar curves which are not shown here), which supports the fact of no interaction between unmodified-TiO_2 and PVDF, responsible for the bad dispersion.

Influence of Dispersion State on the Optical Properties of the Composite Films

CR is the characteristic parameter of the opacity. When the CR reaches 98% the film is completely opaque.[2] Figure 7 displays the effect of pigment dispersion state and PVCs on the CR of the PVDF composite film with a thickness of 20 μm. The CR of PMMA-*g*-TiO_2/PVDF samples was higher than the unmodified-TiO_2/PVDF samples at all experimental pigment concentrations. However, the difference became smaller until the PVCs reached 20%, after which the CR of unmodified-TiO_2/PVDF samples dramatically decreased. The CR increments of both the two systems decreased gradually as the PVCs increased and the increment was even very small during 15%–25% PVCs for the PMMA-*g*-TiO_2/PVDF samples. These results can be explained by the multiple scattering and dependent scattering effect of light. For TiO_2/PVDF system, the opaqueness is only derived from the light scattering by the TiO_2 particles. The mechanism can be shown in the Figure 8(a), for the evenly dispersed system, as the incident light strikes the TiO_2 particle, partial light is reflected for the multiple scattering. As the PVCs increases, the increased scatter centers enhance the multiple scattering, which means higher CR. However, as the PVCs further increases, the reduced inter-particle distance results in the dependent scattering effect and reduces the particle's scattering efficiency. The positive effect of the increased scatter centers will be offset by the decreased scattering efficiency, so the increment of CR decreases. For the unmodified-TiO_2/PVDF samples, TiO_2 particles dispersed in the form of clusters or agglomerations as indicated in the SEM picture [Figure 5(a1,a2)] and modeled in the Figure 8(b). For samples with the same PVCs, the inter-particle distance in the clusters is far smaller than the evenly dispersed samples. The dependent scattering effect take place earlier and stronger for the bad dispersion samples, results in higher CRs for the PMMA-*g*-TiO_2/PVDF samples than the unmodified-TiO_2/PVDF ones. However, as the filling fraction increases, the difference of average inter-particle distance between ideal dispersion and bad dispersion becomes smaller, so the difference of CR decreases. It can be conclude that improving the pigment dispersion plays a greater role for the low PVCs systems than high PVCs ones in enhancing the opacity. The sharp decrease of CR for Vp25 is partly because of the strong dependent scattering, and another important reason is that the whole agglomerate can be seen as a single particle with a lager diameter and much less scattering efficiency for the too small inter-particle distance and even contacted with each other between some particles [as depicted in Figure 8(c)].

The Optical Properties of the CB/PMMA-*g*-TiO_2/PVDF Composite Films

As depicted in Figure 7 that, improving the dispersion of pigment can effectively increase the CR of the composite films.

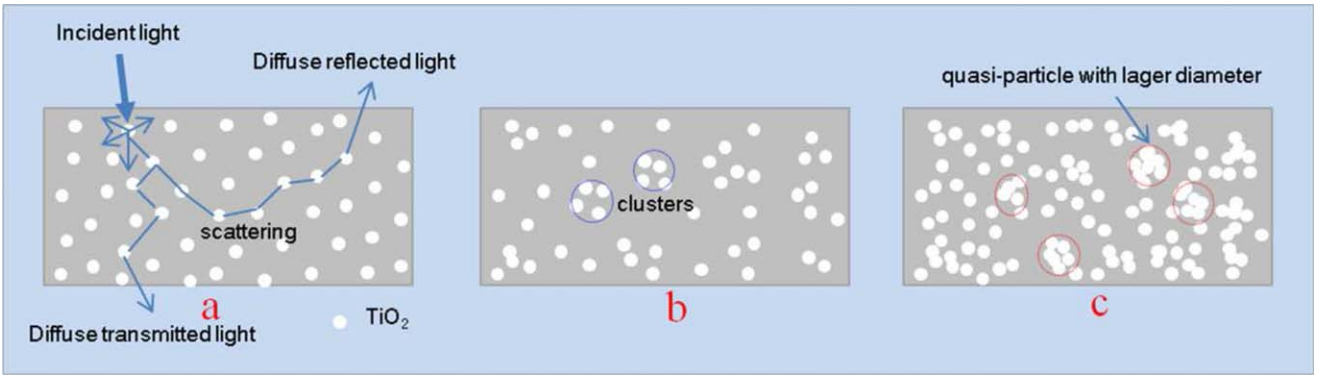

Figure 8. A schematic diagram of the influence of dispersion state on the scattering effect. [Color figure can be viewed in the online issue, which is available at wileyonlinelibrary.com.]

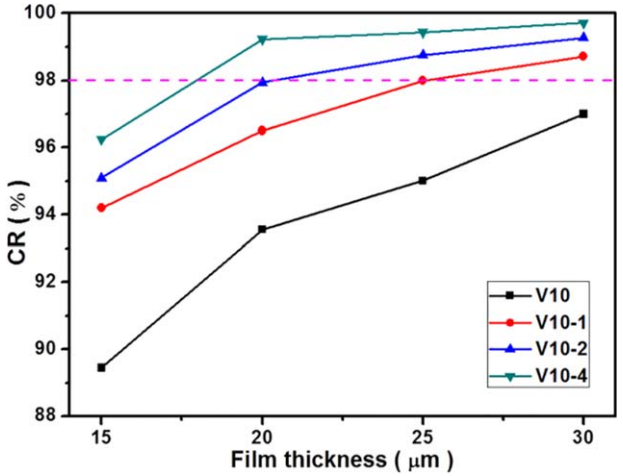

Figure 9. The variation of the CR as a function of the film thickness with different CB concentrations. [Color figure can be viewed in the online issue, which is available at wileyonlinelibrary.com.]

However, no samples exceeded the critical value of 98%. In addition, a further increase of the PVCs had very limited effect on improving the opacity as the PVCs exceeded 10%. Therefore, how to enhance the opacity for a TiO_2 concentration no more than 10% is of great theoretical and practical significance. Few experimental studies concerned the opacity of thin films with both scattering and absorption effect. Figure 9 demonstrated the influence of absorption effect and film thickness on the opacity of the composite films with 10% TiO_2. For the sample of V10 without CB, CR never exceeded 98% at all experimental thickness, but an addition of very small amount of CB remarkably increased the CR. At a constant film thickness, CR increased as a function of enhanced CB concentration. For example, when the concentration of CB was 2×10^{-4} g/cm^3 the CR exceeded 98% for the 20 μm thick film and when the film thickness was greater than 25 μm, only 1×10^{-4} g/cm^3 CB concentration was needed to make CR greater than 98%. This is because that partly light was absorbed by the CB as the light propagating in the film and the transmittance decreased with the CB concentrations increased. Besides, the CR monotonously increased as functions of the film thickness because more light was reflected and absorbed due to the increased amount of scattering and absorption entities as the thickness increased, which resulted in a lower diffuse light transmittance. In the following, the detailed optical properties will be discussed.

Figure 10 shows the reflectance and transmittance spectra of the composite films. The reflectance decreased as the wavelength increased. That's because that the refractive index of TiO_2 decreases with increasing wavelength, which results in the decreased of scattering efficiency and reflectance. Both reflectance and transmittance were weakened with the increasing amount of CB due to the enhanced absorption efficiency. (Samples with different film thickness displayed similar profiles, which were not shown here.)

In order to discuss the influence of CB on the optical properties more deeply, we defined concepts that total diffuse reflectance,

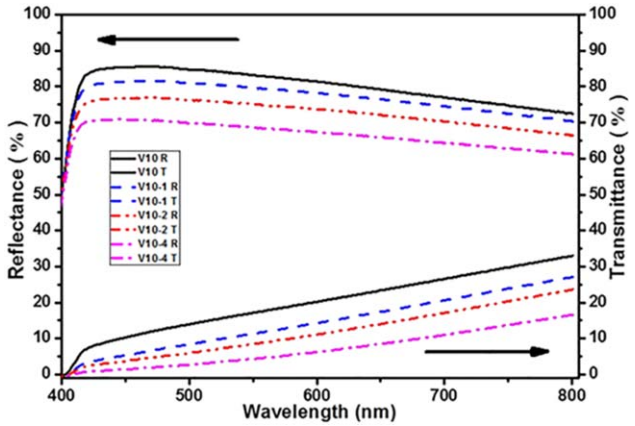

Figure 10. The reflectance and transmittance spectrum of the composite film with different CB concentration at a constant TiO_2 volume concentration 10% and fixed thickness 20 μm. [Color figure can be viewed in the online issue, which is available at wileyonlinelibrary.com.]

total diffuse transmittance and total absorbance. For convenience, we also use the name of reflectance, transmittance, and absorbance henceforth. Reflectance was calculated by the integral area ratio of reflectance spectrum curve against the ideal spectrum curve with 100% reflectance at all wavelengths of visible light (400–800 nm), and the same calculation method was conducted for transmittance. The total absorbance was calculated by subtracting the total reflectance and transmittance from 100%. An inspection into Figures 11 and 12 shows the reflectance, transmittance, and absorptance of the film. At a fixed film thickness, the reflectance and transmittance decreased as the CB concentration increased for the enhancement of the absorptance. As to the samples with the same CB concentration and different thicknesses, the transmittance displayed a monotonous decrease as the thickness increased. That is because the number of scattering and absorbing centers increased as the thickness increased which means more light is reflected and absorbed. Both the enhanced scattering and absorption effect result in the decreased transmittance, as shown in Figure 13 as a schematic illustration of the propagation process of light in

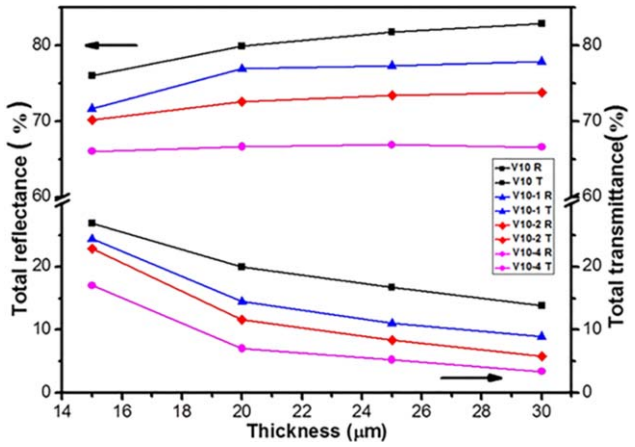

Figure 11. The total reflectance and transmittance as a function of the film thickness with different CB concentrations. [Color figure can be viewed in the online issue, which is available at wileyonlinelibrary.com.]

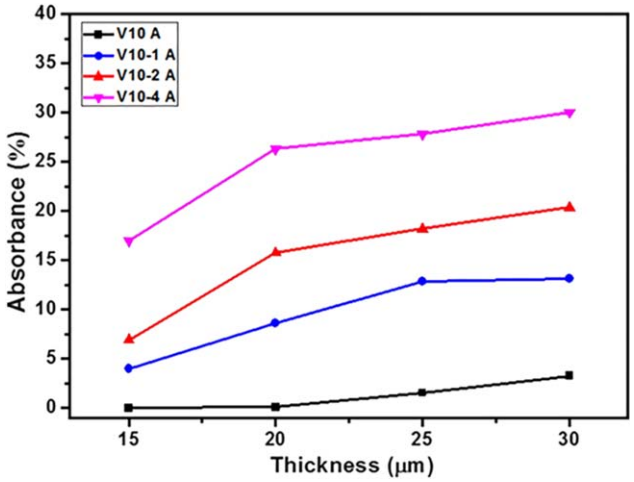

Figure 12. The total absorbance as a function of the film thickness with different CB concentrations. [Color figure can be viewed in the online issue, which is available at wileyonlinelibrary.com.]

the composite film. It is noted that the reflectance process is very complex. When there was no CB, for sample V10, the reflectance increased monotonously as a function of thickness for the increased scattering centers results in more light been reflected. However, the reflectance of V10-1 and V10-2 kept unchanged with the increasing thickness after the thickness exceeded 20 μm. For the sample V10-4, the reflectance was even unchanged at all experimental thickness. This phenomenon can be explained by the compromise between two had contrary effect on the reflectance, that is, multiple scattering and absorption. As shown in Figure 13, the increased thickness means more scattering centers which result in more light propagating backward, however, the increased number of absorbing centers result in more light being absorbed. Therefore, there must be a critical thickness, d_0 (Figure 13). When the thickness is smaller than d_0, as the thickness increased, the enhancement of scattering effects is stronger than the enhancement of absorbing effect,

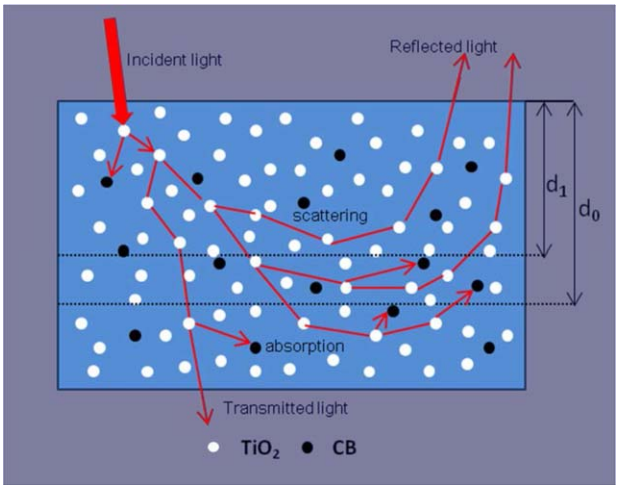

Figure 13. A schematic diagram of light propagating in the composite film. [Color figure can be viewed in the online issue, which is available at wileyonlinelibrary.com.]

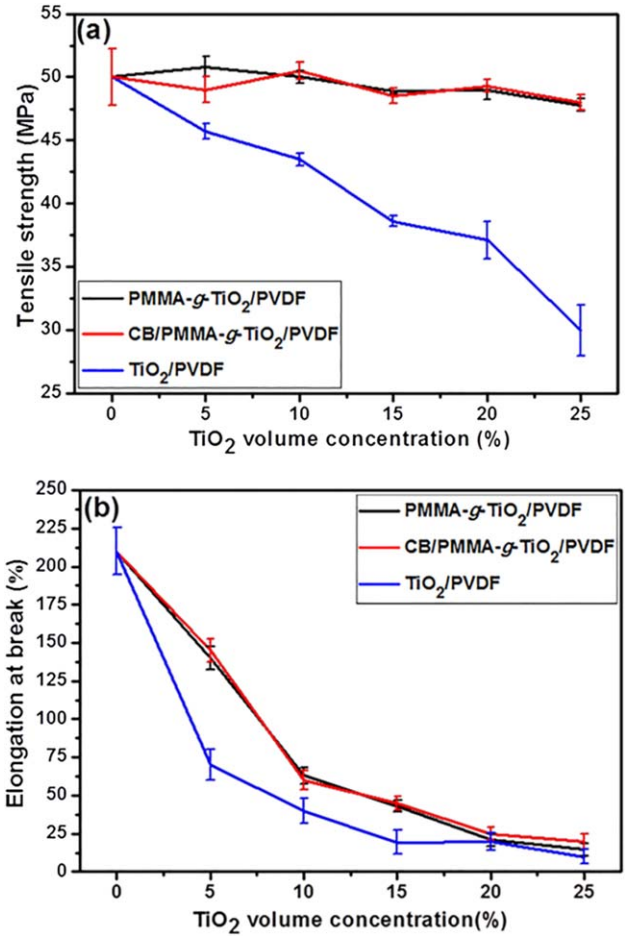

Figure 14. Mechanical properties of PVDF composites film at different TiO_2 concentrations: (a) tensile strength, (b) elongation at break, respectively, specially the CB concentration of the CB/PMMA-g-TiO_2/PVDF samples were 4×10^{-4} g/cm^3. [Color figure can be viewed in the online issue, which is available at wileyonlinelibrary.com.]

so the reflectance increases as the thickness increased, however, the increment of reflectance decreases gradually to zero when the thickness is d_0. Similarly, when the thickness exceeds d_0, the enhancement of scattering effects will be all offset by the absorbing effect. In other words, once the penetration depth of some light exceeds d_0, this part of light could not reach the upper surface of the film to return to the viewer's eyes anymore because of its being completely absorbed by the CB in the propagation process backward. Therefore, the reflectance kept unchanged for a higher thickness. It was clear that a larger CB concentration led to a smaller critical thickness.

The Mechanical Properties of the Composite Films

The mechanical properties of the composite films as a function of volume fraction of TiO_2 are displayed in Figure 14. From the plots in Figure 14(a), it is clear that, the tensile strength of TiO_2/PVDF composite decreased as the TiO_2 concentration increased, conforming to the usual results that incorporation of pigment has negative effect on the mechanical properties of the composites. This can be attributed to the poor TiO_2 dispersion and weak TiO_2/matrix load transfer due to the strong cohesive

forces among the TiO_2 particles and the chemical inertness of the pristine TiO_2 particles inducing weak interfacial adhesion with the polymer matrix. The tensile strength of PMMA-*g*-TiO_2/PVDF systems changed little as the TiO_2 concentration increased. It is because the PMMA, which was anchored to the TiO_2 surface, has excellent miscibility with PVDF due to its specific interaction between the C═O group of PMMA and the CF_2 group of PVDF, it not only improved the dispersion of the TiO_2 particles (as the SEM results displayed) but also enhanced the interfacial adhesion between the TiO_2 and PVDF matrix, both of which results in a more uniform stress distribution and minimizes the presence of stress-concentration centers. As shown in Figure 14(b), the elongation at break decreased as pigment concentration increased both for the TiO_2/PVDF and PMMA-*g*-TiO_2/PVDF samples. However the decrement of PMMA-*g*-TiO_2/PVDF sample was smaller than the TiO_2/PVDF samples as the TiO_2 concentration was lower than 20% for the better load transfer between pigment and PVDF matrix of the modified-TiO_2 system. Trace amount of CB has little effect on the mechanical properties of the composite films, as shown in the Figure 14, the tensile strength and elongation at break of CB/PMMA-*g*-TiO_2/PVDF samples, in which the CB concentration were 4×10^{-4} g/cm^3, were similar to the PMMA-*g*-TiO_2/PVDF samples, because the amount of CB was too small to have any effect on the mechanical properties of the composites.

CONCLUSIONS

Surface graft modification was a useful way to improve pigment dispersion and enhancing the interfacial interaction between the pigment fillers and polymer matrix, which was beneficial to improve the opacity and mechanical properties of the composite films. However, improving the pigment dispersion played a greater role for the low PVCs systems than high PVCs systems on increasing the opacity because of the smaller difference in average inter-particle distance between two types system and the strong dependent scattering effect at high PVCs samples. Adding minute amounts of CB into the PMMA-*g*-TiO_2/PVDF composites could significantly improve the opacity of the composite film based on the combination of the scattering effect and absorbing effect, which can greatly increase the TiO_2 utilization efficiency. It was also found that there was a critical thickness d_0 for the CB/PMMA-*g*-TiO_2/PVDF composite films. The reflectance would increase as the enhanced thickness when the thickness was smaller than d_0, otherwise, the reflectance would keep constant. However, the absorption monotonously increase and the transmittance monotonously decrease as the film thickness increased. In conclusion, a novel method was utilized to manufacture completely opaque white plastic film with relatively lower pigment filling fractions, and both the impact factors and the mechanism were deeply discussed.

ACKNOWLEDGMENTS

This work was supported by the General Armament Department (04060103-7) and (0402030501).

REFERENCES

1. Ross, W. D. *Ind. Eng. Chem. Prod. Res. Dev.* **1974**, *13*, 45.
2. Auger, J. C.; Martinez, V. A.; Stout, B. *J. Coat. Technol. Res.* **2009**, *6*, 89.
3. Auger, J. C.; Stout, B. *J. Coat. Technol. Res.* **2012**, *9*, 287.
4. Thiele, E. S.; French, R. H. *J. Am. Ceram. Soc.* **1998**, *81*, 469.
5. Thiele, E. S.; French, R. H. *Adv. Mater.* **1998**, *10*, 1271.
6. Brown, R. F. G.; Carr, C.; Taylor, M. E. *Prog. Org. Coat.* **1997**, *30*, 195.
7. Veronovski, N.; Lesnik, M.; Verhovsek, D. *J. Coat. Technol. Res.* **2014**, *11*, 255.
8. Karakas, F.; Celik, M. S. *Colloid. Surf. A-Physicochem. Eng. Asp.* **2013**, *434*, 185.
9. Tang, W. H.; Zhu, T. G.; Zhou, P. P.; Zhao, W.; Wang, Q.; Feng, G.; Yuan, H. L. *J. Mater. Sci.* **2011**, *46*, 6656.
10. Maldonado-Valdivia, A. I.; Galindo, E. G.; Ariza, M. J.; Garcia-Salinas, M. *J. Sol. Energy* **2013**, *91*, 263.
11. Carlozzo, B. J. *J. Coat. Technol.* **1997**, *69*, 71.
12. Diebold, M. P. *J. Coat. Technol. Res.* **2011**, *8*, 541.
13. Brown, R. F. G.; Carr, C.; Taylor, M. E. *Prog. Org. Coat.* **1997**, *30*, 185.
14. New Generation, K. -B.; Pigment ExtendersAuger, J. C.; Martinez, V. A.; Stout, B. *J. Coat. Technol. Res.* **2009**, *6*, 89.
15. Zhu, Y.; Allen, G. C.; Adams, J. M.; Gittins, D.; Heard, P. J.; Skuse, D. R. *Compos. Struct.* **2010**, *92*, 2203.
16. Ketpang, K.; Park, J. S. *Synth. Met.* **2010**, *160*, 1603.
17. Chang, C. M.; Hsu, K. Y.; Liu, Y. L. *J. Polym. Sci. Part B: Polym. Phys.* **2012**, *50*, 1151.
18. Mandal, A.; Nandi, A. K. *J. Phys. Chem. C* **2012**, *116*, 9360.
19. Mandal, A.; Nandi, A. K. *J. Mater. Chem.* **2011**, *21*, 15752.
20. Cui, W. W.; Tang, D. Y.; Gong, Z. L. *J. Power Sources* **2013**, *223*, 206.
21. Cao, J.; Wang, L.; He, X. M.; Fang, M.; Gao, J.; Li, J. J.; Deng, L. F.; Chen, H.; Tian, G. Y.; Wang, J. L.; Fan, S. S. *J. Mater. Chem. A* **2013**, *1*, 5955.
22. Mineo, P. G.; Cristaldi, D. A.; Motta, A.; Gupta, T.; Gulino, A. *Rsc Adv.* **2013**, *3*, 1137.
23. Mineo, P.; Motta, A.; Lupo, F.; Renna, L.; Gulino, A. *J. Phys. Chem. C* **2011**, *115*, 12293.
24. Focke, W. W.; Manhique, A.; Carter, R. *J. Am. Ceram. Soc.* **2002**, *85*, 1139.
25. Lee, J. G.; Kim, S. H. *Macromol. Res.* **2011**, *19*, 72.
26. Ma, H. Y.; Xiong, Z. R.; Lv, F. X.; Li, C.; Yang, Y. M. *Macromol. Mater. Eng.* **2012**, *297*, 136.
27. Li, W.; Li, H.; Zhang, Y. M. *J. Mater. Sci.* **2009**, *44*, 2977.
28. Ma, H. Y.; Xiong, Z. R.; Lv, F. X.; Li, C.; Yang, Y. M. *Macromol. Chem. Phys.* **2011**, *212*, 252.
29. Roerdink, E.; Challa, G. *Polymer* **1980**, *21*, 509.
30. Belke, R. E.; Cabasso, I. *Polymer* **1988**, *29*, 1831.
31. Maiti, P.; Nandi, A. K. *Macromolecules* **1995**, *28*, 8511.

32. Briber, R. M.; Khoury, F. *Polymer* **1987**, *28*, 38.
33. Zhao, X. J.; Cheng, J.; Zhang, J.; Chen, S. J.; Wang, X. L. *J. Mater. Sci* **2012**, *47*, 3720.
34. Abolhasani, M. M.; Zarejousheghani, F.; Cheng, Z. X.; Naebe, M. *RSC Adv.* **2015**, *5*, 22471.
35. Hua, H.; Xiong, Y.; Fu, C.; Li, N. *Rsc Adv.* **2014**, *4*, 39273.
36. Al-Ghamdi, G. H.; Sudol, E. D.; Dimonie, V. L.; El-Aasser, M. S. *J. Appl. Polym. Sci.* **2006**, *101*, 2051.
37. Paul, D. R.; Altamirano, J. O. *Adv. Chem. Ser.* **1975**, *142*, 371.
38. Jarray, J.; Larbi, F. B. C.; Vanhulle, F.; Dubault, A.; Halary, J. L. *Macromol. Symp.* **2003**, *198*, 103.
39. Hosoda, T.; Yamada, T. *J. Polym. Eng.* **2013**, *33*, 639.